Superparamagnetic Plasmonic Nanohybrids: Shape-Controlled Synthesis, TEM-Induced Structure Evolution, and Efficient Sunlight-Driven Inactivation of Bacteria

Yueming Zhai, Lei Han, Ping Wang, Gaiping Li, Wen Ren, Ling Liu, Erkang Wang, and Shaojun Dong*

State Key Laboratory of Electroanalytical Chemistry, Changchun Institute of Applied Chemistry, Chinese Academy of Sciences, Graduate School of the Chinese Academy of Sciences, Changchun 130022, Jilin, People's Republic of China

ABSTRACT Magnetic materials and noble metal-based multifunctional hybrids have attracted much attention recently due to their unique properties and potential applications in a variety of fields. However, substantial challenges remain to directly obtain water-soluble hybrids with well-defined structures and to directly combine magnetic nanoparticles with nonspherical noble metals. We describe here for the first time a simple solvothermal method to synthesize a series of novel water-soluble nanohybrids composed of shape-tuned Ag cores and a Fe_3O_4 shell. We found that small Fe_3O_4 grains can be well-distributed directly on the surface on the Ag seeds. Such hybrids have both plasmonic and significant superparamagnetic properties, enabling magnetic separation. The plasmon resonance frequency of Ag nanostructures can be fine-tuned through the interactions between the two components. In addition, the decorated Fe_3O_4 nanoparticles stabilized the Ag nanostructures when exposed to air and natural light for a long time. Furthermore, an interesting structural transformation is observed in the one-dimensional Ag—Fe_3O_4 nanowires under high-energy electron beam. The Ag core can diffuse through the porous iron oxide shell, break away, and result in the formation of Ag nanocluster-decorated iron oxide tubes. Finally, the hybrids acted as a chemical template for the synthesis of Fe_3O_4/Au-AgCl double-layer nanotubes that display obvious near-infrared absorption. Importantly, the double-layer nanotubes exhibited enhanced photocatalytic inactivation of bacteria at very low concentrations under natural sunlight.

KEYWORDS: nanohybrids · iron oxide · silver · superparamagnetic materials · electron-beam irradiation · phototoxicity

Combining multiple components into one nanoparticle (NP) is useful for numerous applications.[1−4] Designing hybrids consisting of various organic and inorganic materials has attracted great attention in the past few years.[5] Materials used range from the inorganic noble metals, carbon nanotubes, graphene, metal oxides, and silica nanowires to small organic molecules and polymers.[6,7] Among the multitude of multicomposites investigated, magnetic materials and noble metal-based hybrids (MNHs) attracted the most attention due to their unique properties demonstrated theoretically and experimentally.[8−12] In terms of catalysis, coupling with magnetic materials enables the nanosized noble metal-based catalysts to be easily recycled by external magnetic field.[11,13] Meanwhile, the contamination of the reaction solution is also avoided. For bioapplications, such as drug delivery,[14] imaging,[15] and therapy,[16,17] MNHs have significant advantages over other hybrids because of the robust interaction between noble metals and thiol groups. Compared to their single-component counterparts, several MNHs have enhanced chemical reactivity and physical properties generated from the interactions between the two components, such as Au—Fe_3O_4,[18] Ag—$CoFe_2O_4$,[19] and Pt—Fe_3O_4.[20]

Up to now, most well-defined structures of MNHs are obtained in nonpolar or low-polar solvents through thermal decomposition of Fe-, Co-, or Ni-based organometallic species and noble metal salts such as dumbbell-like Fe_3O_4—Au,[10] Fe_3O_4—Pt,[20] and Fe_3O_4—Ag,[21] peanut-like Fe_3O_4—Au-PbS,[22] core/shell Fe_3O_4/Au,[23] and core/hollow shell gold/iron oxide at high temperature.[24] However, most applications are carried out in the water phase, and phase transfer is needed through a ligand exchange procedure, especially for biological and environmental use. Additionally, the reagents used (such as organic Fe precursor and solvent with high boiling temperature) are expensive, and especially $Fe(CO)_5$ usually used as a Fe precursor is volatile and toxic. In the water phase, it has been found that direct combination of iron oxide and a noble metal with a well-defined structure is difficult because of their different crystal structures. Flower-like Au—Fe_3O_4 was reported by Yin and co-workers through a bifunctional linker:

* Address correspondence to dongsj@ciac.jl.cn.

Received for review May 22, 2011 and accepted September 27, 2011.

Published online September 28, 2011
10.1021/nn201875k

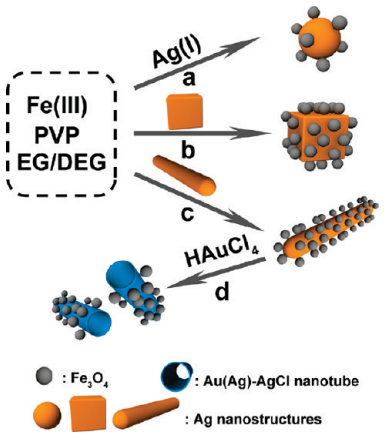

Scheme 1. Schematic depiction of the synthsis of petal-like Ag−Fe_3O_4 (a), Ag nanocube−Fe_3O_4 (b), Ag nanowire−Fe_3O_4 (c), and Fe_3O_4/Au-AgCl nanotube composites (d).

cysteamine.[25] The amine groups react with the carboxyl group on the poly(acrylic acid)-caped Fe_3O_4 nanoparticles, while the thiol groups of cysteamine attach to the surfaces of the gold nanoparticles by the Au−S bond. A common strategy to construct Fe_3O_4/Au or Ag core/shell structures was to modify the Fe_3O_4 nanoparticles first with an amorphous layer (such as SiO_2, polymer, or functional linkers), which can mediate the deposition or assembly of Au or Ag nanoparticles on the magnetic cores.[26−31] Ag−Fe_3O_4 submicrometer composites irregularly doped by Ag and Fe_3O_4 nanoparticles were obtained from solvent-thermal methods in ethylene glycol.[13] Several intrinsic drawbacks exist in these methods, including complicated preparation procedures, nonuniform morphology, and no direct contact, hence no interactions, between a magnetic core and a noble metal shell in most cases. Therefore, new methods are needed to synthesize MNHs in polar systems with well-defined structures, enabling the products to be directly well dispersed in aqueous solution without further modification.

Unlike noble metal nanoparticles with a wide variety of shapes and sizes,[32−34] MNHs are not as well developed. To date, there has been very limited success in nonspherical noble metal-based magnetic hybrids. The properties (such as optical properties) of noble metal nanomaterials are dependent on their size and shape; for example, the plasmon resonance frequencies of Ag nanopheres and Ag nanocubes are different. Many unique properties of noble metals cannot be expected from these MNHs composed of only noble metal nanospheres. Recently, Irudayaraj and co-workers have combined carboxylic Fe_3O_4 NPs and amine-functionalized Au nanorods using EDC/NHS chemistry to construct a multifunctional material with magnetic properties and near-infrared absorption.[16] However, substantial challenges remain to directly deposit magnetic nanoparticles on nonspherical noble metals (such as one-dimensional structures).

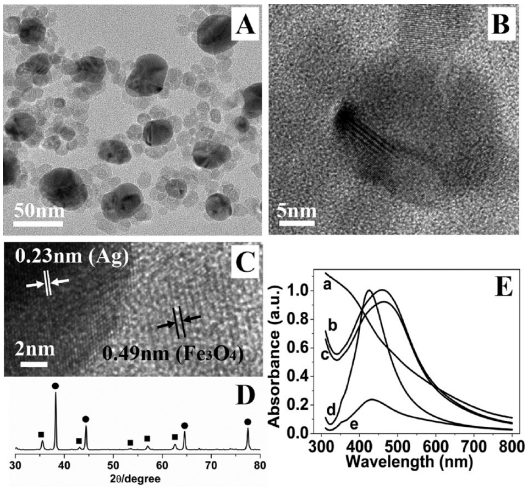

Figure 1. (A and B) Typical TEM graphs of petal-like Ag−Fe_3O_4. (C) High-resolution TEM images of petal-like Ag−Fe_3O_4. (D) XRD patterns of petal-like Ag−Fe_3O_4 (■ Fe_3O_4; ● Ag). (E) UV−vis spectra of the Fe_3O_4 nanoparticles (a), petal-like Ag−Fe_3O_4 (b), petal-like Ag−Fe_3O_4 stored in air and light for 9 days (c), Ag nanoparticles (d), and Ag nanoparticles stored in air and light for 9 days (e).

Herein, we report a new and facile approach for synthesizing water-soluble superparamagnetic bifunctional Ag−Fe_3O_4 hybrids using common materials. A series of Ag nanostructures containing nanospheres, nanocubes, and nanowires were well decorated by Fe_3O_4 NPs. The deposition of Fe_3O_4 could tune the plasmon resonance frequency of the Ag NPs and increase the stability of Ag NPs. Interestingly, under high electron beam, the structure of Ag−Fe_3O_4 nanowires could transform to Ag-decorated nanotubes. Furthermore, the Ag domain had the ability to convert into another noble metal with a hollow cavity and porous walls by the versatile Galvanic reaction. A novel Fe_3O_4/Au-AgCl double-layer nanotube was obtained. Significantly, the nanotubes showed obvious near-infrared absorption and exhibited excellent photocatalytic inactivation of bacteria *via* natural sunlight.

RESULTS AND DISCUSSION

Shape-Tuned Synthesis of Ag−Fe_3O_4 Hybrids. Scheme 1 shows the synthesis steps of magnetic-plasmonic Fe_3O_4−Ag hybrids. The petal-like Ag−Fe_3O_4 nanohybrids were obtained *via* a facile one-pot solvothermal procedure, using silver nitrate and iron nitrate as precursors (Scheme 1a). Figure 1A and B show transmission electron microscopy (TEM) images of the hybrids. Because the electron densities of Ag and Fe_3O_4 NPs differ, the spherical Ag core appeared black and the outer Fe_3O_4 appeared lighter. It can be found that multiple Fe_3O_4 NPs grew on the surface of each Ag NP. The hybrid structure could be seen clearly from the typical high-resolution TEM image (Figure 1C). The distance between two adjacent planes in Fe_3O_4 was 0.49 nm, corresponding to (111) planes of cubic magnetite,[35] and that in Ag was 0.23 nm,

corresponding to (111) planes of fcc structured Ag.[24] Figure 1D showed the XRD result of the composition, which was indexable on the basis of silver (JCPDS No. 87-0720) and magnetite (JCPDS No. 75-1609). Therefore, the formation of hybrids could be confirmed. Absorption spectra of the Fe_3O_4 NPs, Ag NPs, and Ag−Fe_3O_4 NPs in water are shown in Figure 1E. Compared with pure Ag NPs (curve d), the combination with Fe_3O_4 led to a significant red-shift absorption (curve b), indicating the electron changes on the Ag domains due to the interface communication.[10]

It is well known that Ag NPs are unique nanomaterials because of their distinct size- and shape-dependent optical properties.[36] Therefore, we investigated whether our method is applicable to other preformed Ag nanostructures. Ag nanocube−Fe_3O_4 and Ag nanowire−Fe_3O_4 composites were obtained through a seed-mediated approach (Scheme 1b and c). Figure 2A and B are the typical SEM images of the Ag nanocubes and Ag nanocube−Fe_3O_4 hybrids, respectively. It can be observed that the surface of Ag nanocubes became rough after coating with Fe_3O_4 NPs. TEM images (Figure 2C and D) show that Ag nanocubes are surrounded by Fe_3O_4 domains in the hybrids. High-resolution TEM images (Figure 2E) reveal the lattice fringes of Ag and Fe_3O_4. Comparing to the UV−vis absorption spectrum of pure Ag nanocubes (Figure 2F, curve a), a significant red-shift (curve c) was observed for Ag nanocube−Fe_3O_4 hybrids due to component interactions. The compositions of silver and magnetite were also confirmed by XRD (Figure S1a).

Because most of the unique properties of noble metal NPs are associated only with their nanoscale size, preventing aggregation is of particular importance. However, individual Ag NPs can be easily oxidized and gradually form aggregates within several days when exposed to air and light, resulting in a large decrease in intensity of absorption spectra (Figure 1E, curve e and Figure 2F, curve b).[37] In our case, the hybrids were washed with ethanol several times before storing. After at least four months in storage, a certain amount of hybrids were dispersed stably in solution and the sediment could be redispersed well *via* sonication. As shown in Figure 1E, the absorbance intensity of petal-like Ag−Fe_3O_4 nanohybrids (curve c) decreased much less than single Ag NPs (curve e) after storage for 9 days under light. Significantly, no obvious changes in the absorbance spectrum were observed for the Ag nanocube−Fe_3O_4 (Figure 2F, curve d) after 9-day storage under light, demonstrating their excellent stability. Therefore, the hybrids are very stable due to the protection of Fe_3O_4 NPs, which may reduce the oxidation of Ag cores and prevent aggregation by acting as a physical barrier.

The one-dimension Ag−Fe_3O_4 composites were obtained when Ag nanowires were used as seeds. Compared to the pure Ag nanowires shown in Figure 3A,

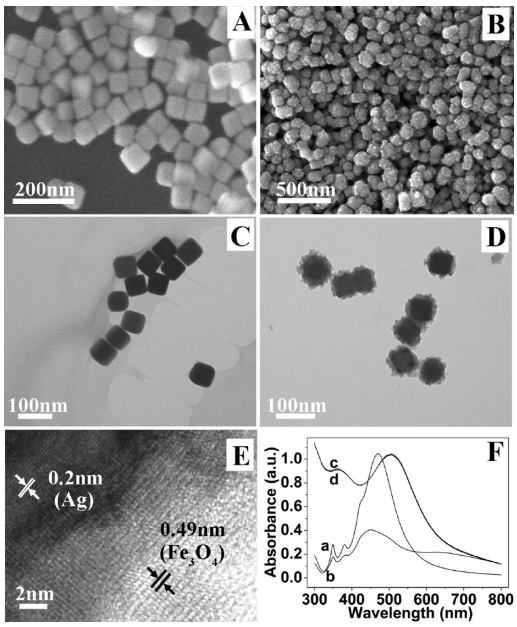

Figure 2. SEM images of Ag nanocubes (A) and Ag nanocube−Fe_3O_4 composites (B). TEM images of Ag nanocubes (C) and Ag nanocube−Fe_3O_4 composites (D). High-resolution TEM images of Ag nanocube−Fe_3O_4 (E). (F) UV−vis spectra of Ag nanocubes (a) and Ag nanocube−Fe_3O_4 (c); Ag nanocubes (b) and Ag nanocube−Fe_3O_4 (d) stored in air and light for 9 days.

hybrids showed a rough surface (Figure 3B and C), revealing the combination of the small Fe_3O_4 NPs. TEM images of Ag nanowires and Ag−Fe_3O_4 nanowires are shown in Figure 3D and E, where the significant changes in surface appearance can be observed. Higher magnification revealed that the wire, including its end (Figure 3E, inset) and side (Figure 3F), was decorated with small Fe_3O_4 NPs. High-resolution TEM images also revealed clearly the crystallization of the Ag and Fe_3O_4 domains (Figure 3G), and the compositions were confirmed by XRD (Figure S1b). The UV−vis spectrum of Ag nanowires shows an asymmetric peak at 404 nm and a small peak at 367 nm (Figure S2a). A perpendicular plasmonic feature is obvious, but the longitudinal resonance is not feasible in the visible range because the nanowire is too long compared with the light wavelength. For Ag nanowire−Fe_3O_4 hybrids, the spectrum shows a peak at 357 nm (Figure S2b), which was overlaid by the absorption of Fe_3O_4 and the Ag nanowire. These results underline one of the key advantages of our approach: different preformed Ag nanostructures may be used as seeds for high-density nucleation of Fe_3O_4.

The magnetic hysteresis loops were measured by a superconducting quantum interference device (SQUID) at 300 K (Figure 4). The saturation magnetizations of petal-like Ag−Fe_3O_4, Ag nanocube−Fe_3O_4, and Ag nanowire−Fe_3O_4 were approximately 19.7, 16.1, and 10.6 emu/g, respectively. Without remnant magnetization, the samples were superparamagnetic

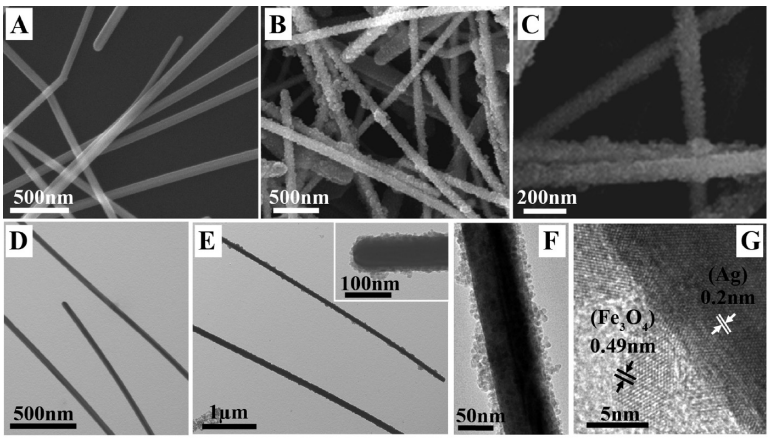

Figure 3. SEM images of Ag nanowires (A) and Ag nanowire−Fe_3O_4 composites (B, C). TEM images of Ag nanowires (D) and Ag nanowire−Fe_3O_4 composites (E, F). High-resolution TEM images of Ag nanowire−Fe_3O_4 (G).

at room temperature. Therefore, the materials could disperse well in solution without magnetic dipole interactions. These measurements also revealed that the hybrids could reach the saturation magnetization easily (below 3000 Oe, easily achieved by an NdFeB magnet). Therefore, the materials are good candidates for magnetic separation, as shown in Figure S3. The BET surface area of Ag nanospheres−Fe_3O_4, Ag nanocubes−Fe_3O_4, and Ag nanowires−Fe_3O_4 were 30.35, 17.75, and 6.14 m^2/g, respectively (Figure S4). It can be found that the surface area decreased with the increasing of the size of Ag cores.

Mechanisms for Hybrid Formation. Although the petal-like Ag−Fe_3O_4 structure was similar to the previously published result when Au NPs were used as seeds for the epitaxial growth of Fe_3O_4 in the slightly polar organic solvent diphenyl ether.[10] Our method has two significant differences from the published method: (1) there are large disparities in solvent polarity used in the two systems as well as iron precursors and capping agents; (2) Fe NPs were formed first on the seeds and transferred to iron oxides in the previously published method, whereas in our method, iron oxides were formed through dehydration of hydrate. Here we propose a possible mechanism for the formation of Ag−Fe_3O_4 hybrids in our method. Ag(I) and Fe(III) can be bound by poly(vinylpyrrolidone) (PVP) used in our method, which donates lone pairs by both nitrogen and oxygen atoms.[13] In the binary solvent system of EG/DEG, Ag(I) and Fe(III) could be reduced to Ag(0) and Fe(II) by the solvent. During heating in the early stage, Ag NPs formed rapidly and PVP was strongly absorbed onto their surface, forming an obstacle for further growth. Because Fe ions can be bound on the Ag NPs by PVP, which acts as a linker, nucleation of Fe_3O_4 may occur *in situ* when the system exceeded a certain temperature. Nucleated Fe_3O_4 may, in turn, serve as seeds for further growth of Fe_3O_4 domains. Rather than forming a continuous Fe_3O_4 shell, multiple small Fe_3O_4 grains

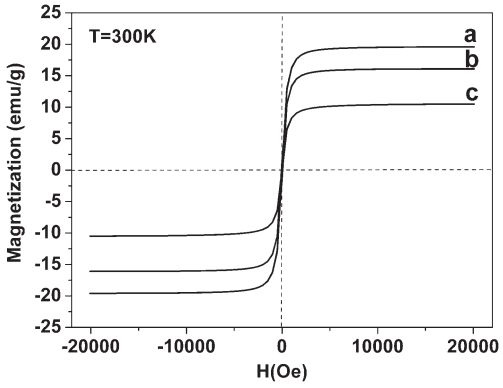

Figure 4. Hysteresis loops of the petal-like Ag−Fe_3O_4 (a), Ag nanocube−Fe_3O_4 (b), and Ag nanowire−Fe_3O_4 composites (c) measured at room temperature.

formed on the polycrystalline Ag seeds along certain facets with low lattice mismatch. The Ag (100) plane (lattice-plane spacing d = 0.20386 nm, JCPDS No. 87-0720) matches the Fe_3O_4 (400) plane (d = 0.20960 nm, JCPDS No. 75-1609) with a mismatch of only 2.74%, and the interfringe distance of the Fe_3O_4 (111) plane (d = 0.48503 nm) is two times that of the Ag (111) plane (d = 0.23540 nm) with a mismatch of 2.93%. Formation of the petral-like hybrid structure is a way to minimize the interfacial area for reducing the interfacial energy.[38] Similar mechanisms could be applied to methods where preformed Ag nanocubes or Ag nanowires protected by PVP were used as seeds.

To investigate the quantity of PVP at the interface of Ag and Fe_3O_4, we moved away these PVP absorbed on Fe_3O_4 through dissolving the Fe_3O_4 domains of the Ag−Fe_3O_4 hybrids by dilute sulfuric acid. The weight percentages of PVP were determined through thermogravimetric analysis (TGA). As shown in Figure S5a, PVP accounts for ~6.47% of the total weight in materials, as derived from the weight losses corresponding to PVP decomposition as the temperature increases. This result proved that there is PVP in the Fe_3O_4−Ag interface, which plays an important role as linker for hybrid

formation. Figure S5b shows that there was more PVP in the Ag nanoparticles directly obtained from the solvothermal method. This may be explained by the fact that high temperature can weaken the surfactant binding to the surface of the Ag seed, leading to loss of some PVP during the synthesis procedure. We also demonstrated that PVP served as a linker in control experiments when additional PVP (1.5 g) was added and preformed Ag nanocubes acted as seeds. Few hybrids were found except separated Ag nanocubes and Fe_3O_4 NPs (data not shown) because Fe(III) bound to much free PVP but not to PVP on the Ag nanocubes. Additionally, we found that the ratio of V_{DEG}/V_{EG} was crucial in generating well-defined Ag−Fe_3O_4 hybrids. When the proportion of DEG increased (V_{DEG}/V_{EG} = 11/1) or when EG was absent, irregular sheet-like Fe_3O_4 structures appeared without obviously combining with Ag (Figure S6). If the proportion of DEG decreased (V_{DEG}/V_{EG} =11/4), a large amount of Fe_3O_4 aggregates occurred with few hybrids being formed (data not shown). In the DEG/EG binary solvent system, increasing the proportion of highly viscous DEG can slow the growth rate of Fe_3O_4, and prevent the formation of large aggregates. However, if only DEG was used, isotropic growth would result in the formation of sheet-like Fe_3O_4.[39]

The stability of preformed Ag nanoseeds during the reaction was found to be critical. Even though Ag(0) can be oxidized by Fe(III), no apparent morphological changes occurred on the Ag nanocubes (Figure 2D) or Ag nanowires (Figure 3E, F) of the hybrids because the solvent effectively prevented Ag(0) from the oxidation.[40] When iron nitrate was replaced by iron chloride and the preformed Ag nanocubes also acted as seeds, a very different result was observed. Apparent deformation of the Ag nanocube was found, although the Fe_3O_4 NPs linked well with the irregular Ag NPs (Figure S7). In the presence of Cl^-, the Ag nanocube was eroded and AgCl formed immediately. AgCl is stable and needs a higher temperature to be reduced back to Ag(0) than Ag ion (or Ag_2O in such an alkaline system) due to the reduced reduction potential from the Ag^+/Ag pair (or Ag_2O/Ag pair) to the AgCl/Ag pair.[41] Through these mechanisms, Cl^- facilitates the dissolution of the Ag nanocubes[42] before the system reaches the temperature for AgCl reduction. These observations indicate that certain iron precursors should be avoided in forming hybrids if the anions in the iron precursors can form an insoluble compound with Ag(I).

TEM-Induced Structural Evolution in Fe_3O_4/Ag Nanowires. Unexpectedly, it was observed that the one-dimensional Ag nanowire−Fe_3O_4 could be transformed *in situ* to nanotubes by etching of the Ag core under electron-beam irradiation. It has been previously reported that the high-energy electron beams in TEM can cause structural changes in some materials.[43,44] For example, Au NPs can coalesce upon exposure to high-energy electron beams.[45] Au(I)-alkanethiolate complexes can be reduced to monodispersed Au NPs by irradiation in TEM.[46] To the best of our knowledge, there have not been previous reports on electron beam-induced structure changes in noble metal/semiconductor-core/shell nanostructures. As shown in Figure 5A, we found that parts of Ag disappeared at some ends of the nanowires during investigation by TEM. When the energy of electron beam irradiation was enhanced (with an accelerating voltage of 100 kV and an electron-gum emission current of 20 μA; a focus area of less than 25 cm^2 on the fluorescent screen), voids appeared on the Ag nanowire immediately and grew larger to form multiple inner channels. After further evolution, the nanotube was formed. The whole process was fast and completed in several seconds. Figure 5B−D show a series of TEM images of the resulting structures. As shown in Figure 5B and C, several segments of Ag stay in the tube. The original Ag core has diffused through the porous iron oxide shell, broke away, and disappeared. Further detailed observation revealed that many small Ag nanoclusters formed stably on the iron oxide shell (Figure 5D). An interesting phenomenon is that once the Ag nanocluster-decorated iron oxide tube formed, the morphology of Ag did not change further over time. A similar process has been reported in a solid-state conversion by Yang and co-workers.[47] ZnO−Au−SiO_2 sandwich nanowires were annealed at 900 °C; then the gold interlayer diffused and was inlaid into the nanotube wall to form a Au NP-decorated nanotube. In our method, the electron-beam irradiation could also impart high energy to the sample.

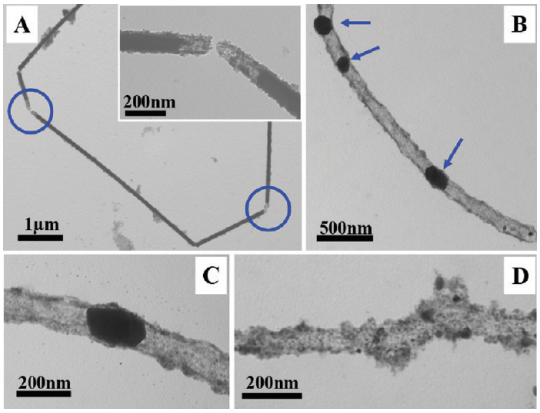

Figure 5. (A) TEM image of Ag nanowire−Fe_3O_4 slightly destroyed by electron-beam irradiation. (B−D) TEM images of Ag nanowire−Fe_3O_4 exposed at high electron beam irradiation.

Electron beam-induced changes in iron oxides (from solid to hollow structure) occurred only in amorphous particles. We did not observe any damages to the iron oxide NPs, suggesting their crystallization. Highly crystalline iron oxide particles are usually stable.[48] However, the final tubes were distorted. The bend of the iron oxide tube may be caused by the rapid movement

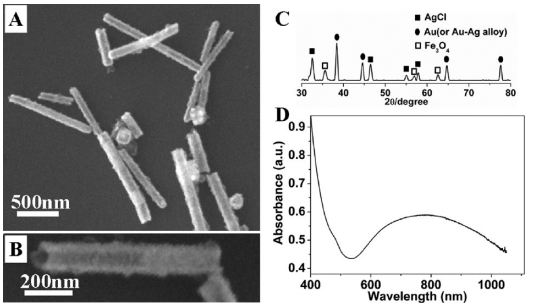

Figure 6. (A, B) SEM images of Fe_3O_4/Au−AgCl nanotubes. (C) XRD patterns of Fe_3O_4/Au−AgCl nanotubes. (D) UV−vis-NIR spectra of Fe_3O_4/Au−AgCl nanotubes.

of Ag in the inner channel and the disappearance of the one-dimension Ag template. These data are useful for solid-state synthesis of novel hybrids by electron-beam irradiation and for methods not involving microscopes such as laser beams and annealing at high temperature.

Synthesis of Derivative Fe_3O_4/Au−AgCl Double-Layer Nanotubes and Their Enhanced Antibacterial Properties under Natural Sunlight. One-dimensional Fe_3O_4/Au−AgCl nanotubes were obtained (Scheme 1d) through Galvanic reaction between Fe_3O_4/Ag nanowires and $HAuCl_4$ since the standard reduction potential of the $AuCl_4^-$/Au pair (0.99 V *vs* SHE) is higher than that of the Ag^+/Ag pair (0.80 V *vs* SHE).[41] Figure 6A presents the SEM image of the nanotubes. It is observed that the original Ag nanowires were broken down to several short segments and had tubular morphology with hollow interiors and opened ends (Figure 6B). XRD patterns showed obvious peaks of AgCl, Au (or Au−Ag alloy), and Fe_3O_4 (Figure 6C). Because the samples used for XRD were collected by magnetic separation during the washing procedure, these coproducts in the galvanic reaction such as free Au nanoclusters and AgCl nanoparticles would be removed. This could be confirmed in the SEM investigation. Comparing to the samples without washing (Figure S8), there were no small irregular nanoclusters besides the hollow hybrids in the sample washed (Figure 6A). Energy-dispersive X-ray spectroscopy (EDS) analyses also demonstrated the presence of Au, Ag, Cl, and Fe elements (Figure S9). These results indicate that the reaction simultaneously precipitated AgCl and Au. Au−Ag alloy may have also formed at the same time by epitaxial depositon of Au on Ag due to their good lattice matching.[41] The absorption spectrum of the hybrid exhibited a major peak in the visible−near-infrared (NIR) region (Figure 6D). Additionally, the hybrid is a good candidate for magnetic separation as shown in Figure S3.

Photocatalysts have attracted tremendous research interest in many years because of their unique applications in the degradation of organic pollutants and the destruction of bacteria.[49,50] Sunlight is the energy source of choice compared to other artificial light. It has been reported that when a semiconductor is combined

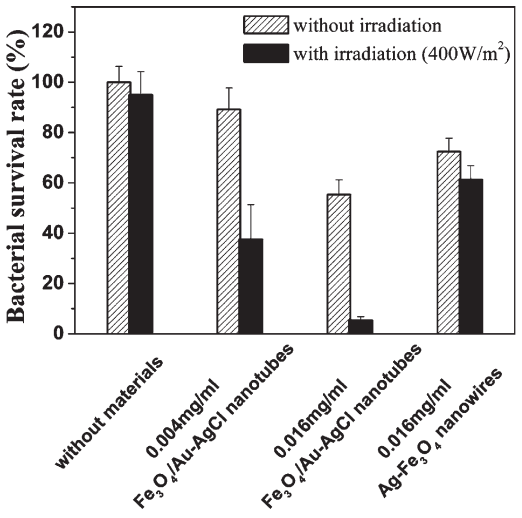

Figure 7. Survival rate of *E. coli* in different treatment conditions. Samples without irradiation were kept in the dark for 40 min, while samples with irradiation were exposed to direct sunlight (400 W/m^2) for 40 min. Sample without hybrids and irradiation was set as the control group with bacterial survival rate 100%. Triplicate experiments were performed in each group. The final values were expressed as a percentage of the control (mean ± standard deviation).

with noble metal NPs, the absorption of visible light can be amplified and the separation process of the photogenerated electrons and holes can be dramatically accelerated.[51] Silver halide/silver or gold plasmonic photocatalysts exhibit efficient photocatalytic activity under visible light irradiation.[52,53] Among the photocatalysts investigated, magnetic photocatalysts have been attracting great attention nowadays due to their ability to magnetically separate.[54,55] Here, we examined the ability of Fe_3O_4/Au−AgCl double-layer nanotubes to destroy bacteria *via* natural sunlight.

The antibacterial activity of the nanotubes against *E. coli*, one of the most important foodborne pathogens, was evaluated by agar plate assays described in the Experimental Section. Figure 7 shows the percentage of viable colonies of *E. coli* in different treatment conditions. Irradiation alone (about 400 W/m^2, 40 min) affected slightly the viability of *E. coli* in the absence of materials. Addition of Fe_3O_4/Au-AgCl nanotubes (0.004 mg/mL) could cause certain inactivation of the *E. coli*. Increasing the amount of Fe_3O_4/Au-AgCl nanotubes to 0.016 mg/mL would cause a higher inactivation rate, so the viable bacteria were reduced significantly in a hybrid concentration-dependent manner. A dramatic enhancement of inactivation efficiency was observed when sunlight irradiation (400 W/m^2, 40 min) was added to the samples containing Fe_3O_4/Au−AgCl nanotubes. Comparing to Fe_3O_4/Au−AgCl nanotubes, Ag−Fe_3O_4 nanowires with the same amount showed lower antibacterial activity, and Ag−Fe_3O_4 nanowires did not show phototoxicity toward *E. coli*. From the nitrogen

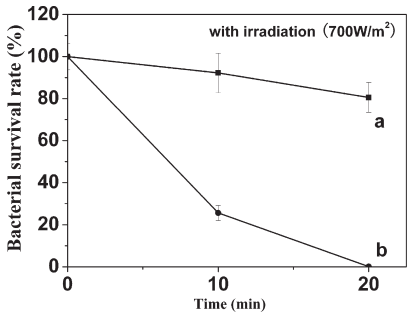

Figure 8. Survival rate of *E. coli* under direct sunlight (700 W/m^2) without hybrids (a) and with 0.016 mg/mL Fe_3O_4/Au−AgCl nanotubes (b).

adsorption−desorption isotherms of Ag−Fe_3O_4 nanowires and Fe_3O_4/Au−AgCl nanotubes (Figure S4), a significant enhancement of the surface area can be found after the hollow structure formed. Low antibacterial activity of Ag−Fe_3O_4 nanowires was possibly due to the low surface area of the Ag structure[56] and the Fe_3O_4 shell attenuating the intrinsic toxicity of silver. Under higher energy sunlight (about 700 W/m^2), the *E. coli* could be completely inactivated in 20 min (Figure 8), while the same intensity of irradiation had little effect on *E. coli* without hybrids. On the basis of the physical and structure characterization above, the excellent photocatalytic activity of Fe_3O_4/Au−AgCl nanotubes could be attributed to the enhanced hole−electron pair generation, as well as good catalytic properties of Au to produce radical species. The tube-like structure is also favorable for utilization of the light because light may be reflected repeatedly in the tube. The tubes were composed of a thin complex layer of AgCl, Au, and Ag. Au nanoparticles combined with AgCl should polarize its electron distribution. In the hybrids, the negative regions were far from the Au/AgCl interface, while positive regions were close to the Au/AgCl interface. The surface plasmon resonance of the Au nanoparticles lies in the visible region, which is favorable to photocatalytic reaction driven by visible light. Under sunlight irradiation, an absorbed photon would be efficiently separated into an electron and a hole at the Au domains. The excellent conductivity of Au nanoparticles can enhance the electron translation and the interfacial charge transfer. The recombination of electron−hole pairs was reduced efficiently. The photogenerated electrons could transfer to the present molecular oxygen in the solution to form active species such as $O_2^{-\bullet}$.[57] At the same time, the holes transfer to the surface of the AgCl particle, which contains Cl^-. Holes could oxidize Cl^- ions to Cl^0.[53] The formed chlorine atoms and oxygen species are all reactive radical species, which, in turn, could effectively destroy the bacteria.

CONCLUSION

In summary, a novel protocol has been developed for synthesizing magnetic−plasmonic Ag−Fe_3O_4 hybrids with different morphologies. The petal-like Ag−Fe_3O_4 nanohybrids were obtained *via* a simple one-pot solvent thermal procedure, and hybrids consisting of other Ag nanostructures were synthesized by a seed-mediated process. It has been experimentally proved that both binary solvent EG/DEG and PVP played important roles for the well-defined hybrid structures. The addition of Fe_3O_4 NPs stabilized the Ag core. The Fe_3O_4/Ag nanowire could transform into a Ag nanocluster-decorated iron oxide nanotube under high electron-beam irradiation, which may provide a new approach for solid-state synthesis of hybrids. A novel structure of Fe_3O_4/Au−AgCl double-layer nanotubes was obtained through galvanic reaction. The nanotubes demonstrated excellent bactericidal activity *via* natural sunlight. Our solvent thermal protocol may be applicable in generating various water-soluble MNHs with different compositions and morphologies by simply supplying different seeds for certain applications and systematically studying the interactions on noble metal−iron oxide composites.

EXPERIMENTAL SECTION

Reagents. Ferric chloride, ferric nitrate, ethylene glycol, diethylene glycol, sodium acetate anhydrous, silver nitrate, sodium sulfide, poly(vinylpyrrolidone) (average M_w = 40 000), and $HAuCl_4$ were purchased from Beijing Chemical Reagent Factory (Beijing, China). All reagents were used as received without further purification. The water used was purified through a Millipore system. *E. coli* was obtained from Kunming Institute of Zoology, Chinese Academy of Sciences.

Preparation of Ag−Fe_3O_4 Hybrids. Ferric nitrate (0.12 g) was dissolved in a mixture (14 mL) of ethylene glycol and diethylene glycol (volume ratio 3:11) containing sodium acetate anhydrous (1 g) and PVP (1.5 g) to form a homogeneous solution by vigorous stirring and heat, purged with N_2 for 50 min. Then silver nitrate (0.025 g) was added, and the mixture was sealed in a Teflon-lined stainless-steel autoclave. The autoclave was heated to and maintained at 200 °C for 10 h and allowed to cool to room temperature. The products were washed several times with ethanol and dried at 60 °C.

Preparation of Ag Nanopartides. Silver nitrate (0.1 g) was dissolved in a mixture (14 mL) of ethylene glycol and diethylene glycol (volume ratio 3:11) containing PVP (1.5 g). The mixture was purged with N_2 for 50 min and then sealed in a Teflon-lined stainless-steel autoclave, maintained at 200 °C for 10 h, and allowed to cool to room temperature. The products were washed several times with ethanol.

Preparation of Ag−Fe_3O_4 Hybrids with Supplied Ag Seeds. Ag nanocubes and Ag nanowires were obtained from procedures reported by Xia and co-workers.[58,59] A 3 mL amount ethylene glycol containing Ag nanocubes or Ag nanowires was added to 11 mL of diethylene glycol containing ferric nitrate (0.03 g) and sodium acetate anhydrous (1 g), which was made homogeneously by vigorous stirring and heat under N_2 flow for 50 min. The mixture was sealed in a Teflon-lined stainless-steel autoclave, then maintained at 200 °C for 10 h. The products were washed several times with ethanol and dispersed in 15 mL of water.

Preparation of Fe_3O_4/Au−AgCl Nanotubes. A 0.5 mL portion of the above solution containing Ag−Fe_3O_4 nanowires was added to

10 mL of aqueous solution containing 50 mg of PVP, purged with N_2 for 50 min, and kept in a 50 °C water bath. Then 3 mL of 0.16 mM $HAuCl_4$ aqueous solution was added to the mixture under vigorous mechanical stirring and reacted for 20 min. The products were separated with a magnet and washed with water at least three times.

Instruments. A XL30E SEM scanning electron microscope equipped with an energy-dispersive X-ray analyzer was used to determine the composition of the products. SEM images were taken on a JEOL JXA-840 scanning microanalyzer scanning electron microscope, and the accelerating voltage was 20 kV. UV−vis−NIR spectra were collected on a CARY 500 Scan UV−vis−NIR spectrophotometer. All samples were treated by short sonication before measurement. TEM measurements were made on a Hitachi H-8100 EM with an accelerating voltage of 100 kV and a FEI-TECNAI G^2 transmission electron microscope operating at 200 kV. X-ray diffraction (XRD) analysis was carried out on a D/Max 2500 V/PC X-ray diffractometer using Cu (40 kV, 30 mA) radiation. Magnetic measurements were carried out using a superconducting quantum interference device (SQUID) magnetometer (LakeShore 7307) at 300 K. The SQUID measurements for all the samples were done on the pure and dried powders. The intensity of sunlight was measured by a solar power meter (TES 1333). Nitrogen adsorption−desorption isotherms at the temperature of liquid nitrogen were measured by using a Micromeritics ASAP 2010 analyzer (USA) with nitrogen. The samples were degassed under vacuum for 4 h at 160 °C before the measurements. TGA was conducted on a Perkin-Elmer thermal analyzer from room temperature to 700 °C with a heating rate of 10 °C min^{-1} in the nitrogen flow.

Antibacterial Activity against *E. coli*. *E. coli* was used in this study. The bacteria were grown aerobically at 37 °C for 12 h on a rotary shaker in Luria broth medium. After being properly diluted (500-fold), 80 μL aliquots of the bacterial suspension were mixed with 2 mL of composites solution. A 10 μL sample of each mixture was spread on the agar plates after the specific treatment, and the plates were inverted and incubated at 37 °C for 20 h. All measurements were performed in triplicate. The photograph of colonies of *E. coli* incubated on agar plates was taken by a camera, and the number of colonies was counted exactly to determine the antibacterial activity.

Acknowledgment. This work was supported by the National Natural Science Foundation of China (Nos. 20820102037 and 20935003) and National Basic Research Program of China (973 program; Nos. 2010CB933600 and 2009CB930100)

Supporting Information Available: Additional characterization data for hybrids (XRD analysis, UV−vis spectra, photographs, N_2 adsorption−desorption isotherms, TGA curves, TEM images, SEM image, and EDS spectra). This material is available free of charge *via* the Internet at http://pubs.acs.org.

REFERENCES AND NOTES

1. Costi, R.; Saunders, A. E.; Banin, U. Colloidal Hybrid Nanostructures: A New Type of Functional Materials. *Angew. Chem., Int. Ed.* **2010**, *49*, 4878–4897.
2. Xu, C.; Xie, J.; Ho, D.; Wang, C.; Kohler, N.; Walsh, E. G.; Morgan, J. R.; Chin, Y. E.; Sun, S. Au-Fe_3O_4 Dumbbell Nanoparticles as Dual-Functional Probes. *Angew. Chem., Int. Ed.* **2008**, *47*, 173–176.
3. Jin, Y. D.; Gao, X. H. Plasmonic Fluorescent Quantum Dots. *Nat. Nanotechnol.* **2009**, *4*, 571–576.
4. Bardhan, R.; Chen, W. X.; Bartels, M.; Perez-Torres, C.; Botero, M. F.; McAninch, R. W.; Contreras, A.; Schiff, R.; Pautler, R. G.; Halas, N. J.; Joshi, A. Tracking of Multimodal Therapeutic Nanocomplexes Targeting Breast Cancer in Vivo. *Nano Lett.* **2010**, *10*, 4920–4928.
5. Xiao, Y. H.; Li, C. M. Nanocomposites: From Fabrications to Electrochemical Bioapplications. *Electroanalysis* **2008**, *20*, 648–662.
6. Chen, W.; Li, C. M.; Yu, L.; Lu, Z. S.; Zhou, Q. *in situ* AFM Study of Electrochemical Synthesis of Polypyrrole/Au Nanocomposite. *Electrochem. Commun.* **2008**, *10*, 1340–1343.
7. Yuan, W. Y.; Li, C. M. Direct Modulation of Localized Surface Plasmon Coupling of Au Nanoparticles on Solid Substrates *via* Weak Polyelectrolyte-Mediated Layer-by-Layer Self Assembly. *Langmuir* **2009**, *25*, 7578–7585.
8. Levin, C. S.; Hofmann, C.; Ali, T. A.; Kelly, A. T.; Morosan, E.; Nordlander, P.; Whitmire, K. H.; Halas, N. J. Magnetic-Plasmonic Core-Shell Nanoparticles. *ACS Nano* **2009**, *3*, 1379–1388.
9. Lu, Y.; Shi, C.; Hu, M. J.; Xu, Y. J.; Yu, L.; Wen, L. P.; Zhao, Y.; Xu, W. P.; Yu, S. H. Magnetic Alloy Nanorings Loaded with Gold Nanoparticles: Synthesis and Applications as Multimodal Imaging Contrast Agents. *Adv. Funct. Mater.* **2010**, *20*, 3701–3706.
10. Yu, H.; Chen, M.; Rice, P. M.; Wang, S. X.; White, R. L.; Sun, S. H. Dumbbell-Like Bifunctional Au-Fe_3O_4 Nanoparticles. *Nano Lett.* **2005**, *5*, 379–382.
11. Shylesh, S.; Schunemann, V.; Thiel, W. R. Magnetically Separable Nanocatalysts: Bridges between Homogeneous and Heterogeneous Catalysis. *Angew. Chem., Int. Ed.* **2010**, *49*, 3428–3459.
12. McKiernan, M.; Zeng, J.; Ferdous, S.; Verhaverbeke, S.; Leschkies, K. S.; Gouk, R.; Lazik, C.; Jin, M.; Briseno, A. L.; Xia, Y. N. Facile Synthesis of Bimetallic Ag/Ni Core/Sheath Nanowires and Their Magnetic and Electrical Properties. *Small* **2010**, *6*, 1927–1934.
13. Zhang, D. H.; Li, G. D.; Li, J. X.; Chen, J. S. One-pot Synthesis of Ag-Fe_3O_4 Nanocomposite: A Magnetically Recyclable and Efficient Catalyst for Epoxidation of Styrene. *Chem. Commun.* **2008**, 3414–3416.
14. Xu, C. J.; Wang, B. D.; Sun, S. H. Dumbbell-like Au-Fe_3O_4 Nanoparticles for Target-Specific Platin Delivery. *J. Am. Chem. Soc.* **2009**, *131*, 4216–4217.
15. Jiang, J.; Gu, H. W.; Shao, H. L.; Devlin, E.; Papaefthymiou, G. C.; Ying, J. Y. Manipulation Bifunctional Fe_3O_4-Ag Heterodimer Nanoparticles for Two-Photon Fluorescence Imaging and Magnetic Manipulation. *Adv. Mater.* **2008**, *20*, 4403–4407.
16. Wang, C. G.; Chen, J.; Talavage, T.; Irudayaraj, J. Gold Nanorod/Fe_3O_4 Nanoparticle "Nano-Pearl-Necklaces" for Simultaneous Targeting, Dual-Mode Imaging, and Photothermal Ablation of Cancer Cells. *Angew. Chem., Int. Ed.* **2009**, *48*, 2759–2763.
17. Chen, W.; Xu, N. F.; Xu, L. G.; Wang, L. B.; Li, Z. K.; Ma, W.; Zhu, Y. Y.; Xu, C. L.; Kotov, N. A. Multifunctional Magnetoplasmonic Nanoparticle Assemblies for Cancer Therapy and Diagnostics (Theranostics). *Macromol. Rapid Commun.* **2010**, *31*, 228–236.
18. Lee, Y. M.; Garcia, M. A.; Huls, N. A. F.; Sun, S. H. Synthetic Tuning of the Catalytic Properties of Au-Fe_3O_4 Nanoparticles. *Angew. Chem., Int. Ed.* **2010**, *49*, 1271–1274.
19. Li, Y. Q.; Zhang, G.; Nurmikko, A. V.; Sun, S. H. Enhanced Magnetooptical Response in Dumbbell-like Ag-$CoFe_2O_4$ Nanoparticle Pairs. *Nano Lett.* **2005**, *5*, 1689–1692.
20. Wang, C.; Daimon, H.; Sun, S. H. Dumbbell-like Pt-Fe_3O_4 Nanoparticles and Their Enhanced Catalysis for Oxygen Reduction Reaction. *Nano Lett.* **2009**, *9*, 1493–1496.
21. Wang, C.; Yin, H. F.; Dai, S.; Sun, S. H. A General Approach to Noble Metal-Metal Oxide Dumbbell Nanoparticles and Their Catalytic Application for CO Oxidation. *Chem. Mater.* **2010**, *22*, 3277–3282.
22. Shi, W. L.; Zeng, H.; Sahoo, Y.; Ohulchanskyy, T. Y.; Ding, Y.; Wang, Z. L.; Swihart, M.; Prasad, P. N. A General Approach to Binary and Ternary Hybrid Nanocrystals. *Nano Lett.* **2006**, *6*, 875–881.
23. Wang, L. Y.; Luo, J.; Fan, Q.; Suzuki, M.; Suzuki, I. S.; Engelhard, M. H.; Lin, Y. H.; Kim, N.; Wang, J. Q.; Zhong, C. J. Monodispersed Core-shell Fe_3O_4@Au Nanoparticles. *J. Phys. Chem. B* **2005**, *109*, 21593–21601.
24. Shevchenko, E. V.; Bodnarchuk, M. I.; Kovalenko, M. V.; Talapin, D. V.; Smith, R. K.; Aloni, S.; Heiss, W.; Alivisatos, A. P. Gold/Iron Oxide Core/Hollow-Shell Nanoparticles. *Adv. Mater.* **2008**, *20*, 4323–4329.
25. Ge, J. P.; Hu, Y. X.; Biasini, M.; Dong, C. L.; Guo, J. H.; Beyermann, W. P.; Yin, Y. D. One-Step Synthesis of Highly Water-Soluble Magnetite Colloidal Nanocrystals. *Chem.—Eur. J.* **2007**, *13*, 7153–7161.

26. Ling, B.; Wen, Y.; Yu, Z. Q.; Yu, Y. H.; Yang, H. F. Multifunctional Magnetic Nanocomposites: Separation, Photodecomposition and Raman Detection. *J. Mater. Chem.* **2011**, *21*, 4623–4628.
27. Guo, S.; Dong, S.; Wang, E. A General Route to Construct Diverse Multifunctional Fe_3O_4/Metal Hybrid Nanostructures. *Chem.—Eur. J.* **2009**, *15*, 2416–2424.
28. Bao, J.; Chen, We.; Liu, T. T.; Zhu, Y. L.; Jin, P. Y.; Wang, L. Y.; Liu, J. F.; Wei, Y. G.; Li, Y. D. Bifunctional Au-Fe_3O_4 Nanoparticles for Protein Separation. *ACS Nano* **2007**, *1*, 293–298.
29. Wang, L. Y.; Bai, J. W.; Li, Y. J.; Huang, Y. Multifunctional Nanoparticles Displaying Magnetization and Near-IR Absorption. *Angew. Chem., Int. Ed.* **2008**, *47*, 2439–2442.
30. Salgueirino-Maceira, V.; Correa-Duarte, M. A.; Farle, M.; Lopez-Quintela, A.; Sieradzki, K.; Diaz, R. Bifunctional Gold-Coated Magnetic Silica Spheres. *Chem. Mater.* **2006**, *18*, 2701–2706.
31. Zhai, Y. M.; Zhai, J. F.; Wang, Y. L.; Guo, S. J.; Ren, W.; Dong, S. J. Fabrication of Iron Oxide Core/Gold Shell Submicrometer Spheres with Nanoscale Surface Roughness for Efficient Surface-Enhanced Raman Scattering. *J. Phys. Chem. C* **2009**, *113*, 7009–7014.
32. Xia, Y.; Xiong, Y. J.; Lim, B.; Skrabalak, S. E. Shape-Controlled Synthesis of Metal Nanocrystals: Simple Chemistry Meets Complex Physics? *Angew Chem., Int. Ed.* **2009**, *48*, 60–103.
33. Sau, T. K.; Rogach, A. L. Nonspherical Noble Metal Nanoparticles: Colloid-Chemical Synthesis and Morphology Control. *Adv. Mater.* **2010**, *22*, 1781–1804.
34. Tao, A. R.; Habas, S.; Yang, P. D. Shape Control of Colloidal Metal Nanocrystals. *Small* **2008**, *4*, 310–325.
35. Ge, J. P.; Hu, Y. X.; Biasini, M.; Beyermann, W. P.; Yin, Y. D. Superparamagnetic Magnetite Colloidal Nanocrystal Clusters. *Angew. Chem., Int. Ed.* **2007**, *46*, 4342–4345.
36. Wiley, B.; Sun, Y. G.; Xia, Y. Synthesis of Silver Nanostructures with Controlled Shapes and Properties. *Acc. Chem. Res.* **2007**, *40*, 1067–1076.
37. Lv, M.; Su, S.; He, Y.; Huang, Q.; Hu, W.; Li, D.; Fan, C.; Lee, S. T. Long-Term Antimicrobial Effect of Silicon Nanowires Decorated with Silver Nanoparticles. *Adv. Mater.* **2010**, *22*, 5463–5467.
38. Carbone, L.; Cozzoli, P. D. Colloidal Heterostructured Nanocrystals: Synthesis and Growth Mechanisms. *Nano Today* **2010**, *5*, 449–493.
39. Xuan, S. H.; Wang, F.; Wang, Y. X. J.; Yu, J. C.; Leung, K. C. F. Facile Synthesis of Size-Controllable Monodispersed Ferrite Nanospheres. *J. Mater. Chem.* **2010**, *20*, 5086–5094.
40. Wiley, B.; Sun, Y. G.; Xia, Y. N. Polyol Synthesis of Silver Nanostructures: Control of Product Morphology with Fe (II) or Fe (III) Species. *Langmuir* **2005**, *21*, 8077–8080.
41. Sun, Y. G. Silver Nanowires−Unique Templates for Functional Nanostructures. *Nanoscale* **2010**, *2*, 1626–1642.
42. Wiley, B.; Herricks, T.; Sun, Y. G.; Xia, Y. N. Polyol Synthesis of Silver Nanoparticles: Use of Chloride and Oxygen to Promote the Formation of Single-Crystal, Truncated Cubes and Tetrahedrons. *Nano Lett.* **2004**, *4*, 1733–1739.
43. Latham, A. H.; Wilson, M. J.; Schiffer, P.; Williams, M. E. TEM-Induced Structural Evolution in Amorphous Fe Oxide Nanoparticles. *J. Am. Chem. Soc.* **2006**, *128*, 12632–12633.
44. Smith, D. J.; Petfordlong, A. K.; Wallenberg, L. R.; Bovin, J. O. Dynamic Atomic-Level Rearrangements in Small Gold Particles. *Science* **1986**, *233*, 872–875.
45. Jose-Yacaman, M.; Gutierrez-Wing, C.; Miki, M.; Yang, D. Q.; Piyakis, K. N.; Sacher, E. Surface Diffusion and Coalescence of Mobile Metal Nanoparticles. *J. Phys. Chem. B* **2005**, *109*, 9703–9711.
46. Kim, J. U.; Cha, S. H.; Shin, K.; Jho, J. Y.; Lee, J. C. Synthesis of Gold Nanoparticles from Gold(I)-alkanethiolate Complexes with Supramolecular Structures Through Electron Beam Irradiation in TEM. *J. Am. Chem. Soc.* **2005**, *127*, 9962–9963.
47. Yang, Y.; Yang, R. B.; Fan, H. J.; Scholz, R.; Huang, Z.; Berger, A.; Qin, Y.; Knez, M.; Gösele, U. Diffusion-Facilitated Fabrication of Gold-Decorated Zn_2SiO_4 Nanotubes by a One-Step Solid-State Reaction. *Angew. Chem., Int. Ed.* **2010**, *49*, 1442–1446.
48. Latham, A. H.; Williams, M. E. Transmission Electron Microscope-Induced Structural Evolution in Amorphous Fe, Co, and Ni Oxide Nanoparticles. *Langmuir* **2008**, *24*, 14195–14202.
49. Linsebigler, A. L.; Lu, G.; Yates, J. T. Photocatalysis on TiO_2 Surfaces: Principles, Mechanisms, and Selected Results. *Chem. Rev.* **1995**, *95*, 735–758.
50. Lan, Y. Q.; Hu, C.; Hu, X. X.; Qu, J. H. Efficient Destruction of Pathogenic Bacteria with AgBr/TiO_2 under Visible Light Irradiation. *Appl. Catal., B* **2007**, *73*, 354–360.
51. Chen, X.; Zhu, H. Y.; Zhao, J. C.; Zheng, Z. T.; Gao, X. P. Visible-Light-Driven Oxidation of Organic Contaminants in Air with Gold Nanoparticle Catalysts on Oxide Supports. *Angew. Chem., Int. Ed.* **2008**, *47*, 5353–5356.
52. An, C. H.; Peng, S. N.; Sun, Y. G. Facile Synthesis of Sunlight-Driven AgCl:Ag Plasmonic Nanophotocatalyst. *Adv. Mater.* **2010**, *22*, 2570–2574.
53. Wang, P.; Huang, B. B.; Qin, X. Y.; Zhang, X. Y.; Dai, Y.; Wei, J. Y.; Whangbo, M. H. Ag@AgCl: A Highly Efficient and Stable Photocatalyst Active under Visible Light. *Angew. Chem., Int. Ed.* **2008**, *47*, 7931–7933.
54. Chen, W. J.; Chen, Y. C. Fe_3O_4/TiO_2 Core/shell Magnetic Nanoparticle-based Photokilling of Pathogenic Bacteria. *Nanomedicine (London)* **2010**, *5*, 1585–1593.
55. Ye, M. M.; Zhang, Q.; Hu, Y. X.; Ge, J. P.; Lu, Z. D.; He, L.; Chen, Z. L.; Yin, Y. D. Magnetically Recoverable Core-Shell Nanocomposites with Enhanced Photocatalytic Activity. *Chem.—Eur. J.* **2010**, *16*, 6243–6250.
56. Pang, M. L.; Hu, J. Y.; Zeng, H. C. Synthesis, Morphological Control, and Antibacterial Properties of Hollow/Solid Ag_2S/Ag Heterodimers. *J. Am. Chem. Soc.* **2010**, *132*, 10771–10785.
57. Yu, J.; Dai, G.; Huang, B. Fabrication and Characterization of Visible-Light-Driven Plasmonic Photocatalyst Ag/AgCl/TiO_2 Nanotube Arrays. *J. Phys. Chem. C* **2009**, *113*, 16394–16401.
58. Siekkinen, A. R.; McLellan, J. M.; Chen, J. Y.; Xia, Y. N. Rapid Synthesis of Small Silver Nanocubes by Mediating Polyol Reduction with a Trace Amount of Sodium Sulfide or Sodium Hydrosulfide. *Chem. Phys. Lett.* **2006**, *432*, 491–496.
59. Sun, Y. G.; Yin, Y. D.; Mayers, B. T.; Herricks, T.; Xia, Y. N. Uniform Silver Nanowires Synthesis by Reducing $AgNO_3$ with Ethylene Glycol in the Presence of Seeds and Poly(vinyl pyrrolidone). *Chem. Mater.* **2002**, *14*, 4736–4745.